CrossMark

ELSEVIER

http://dx.doi.org/10.1016/j.ultrasmedbio.2016.09.011

● **Original Contribution**

CHARACTERISATION OF LIPOSOME-LOADED MICROBUBBLE POPULATIONS FOR SUBHARMONIC IMAGING

JAMES R. MCLAUGHLAN,[*†] SEVAN HARPUT,[*] RADWA H. ABOU-SALEH,[‡§] SALLY A. PEYMAN,[‡] STEPHEN EVANS,[‡] and STEVEN FREEAR[*]

*School of Electronic and Electrical Engineering, University of Leeds, Leeds, UK; †Division of Biomedical Imaging, University of Leeds, Leeds, UK; ‡School of Physics and Astronomy, University of Leeds, Leeds, UK; and §Department of Physics, Faculty of Science, Mansoura University, Mansoura City, Egypt

Abstract—Therapeutic microbubbles could make an important contribution to the diagnosis and treatment of cancer. Acoustic characterisation was performed on microfluidic generated microbubble populations that either were bare or had liposomes attached. Through the use of broadband attenuation techniques (3–8 MHz), the shell stiffness was measured to be 0.72 ± 0.01 and 0.78 ± 0.05 N/m and shell friction was 0.37 ± 0.05 and $0.74 \pm 0.05 \times 10^{-6}$ kg/s for bare and liposome-loaded microbubbles, respectively. Acoustic scatter revealed that liposome-loaded microbubbles had a lower subharmonic threshold, occurring from a peak negative pressure of 50 kPa, compared with 200 kPa for equivalent bare microbubbles. It was found that liposome loading had a negligible effect on the destruction threshold for this microbubble type, because at a mechanical index >0.4 (570 kPa), 80% of both populations were destroyed. (E-mail: j.r.mclaughlan@leeds.ac.uk)   © 2016 The Authors. Published by Elsevier Inc. on behalf of World Federation for Ultrasound in Medicine & Biology. This is an open access article under the CC BY license (http://creativecommons.org/licenses/by/4.0/).

Key Words: Ultrasound contrast agents, Drug delivery, Subharmonic imaging, Microfluidics, Liposomes, Microbubbles.

INTRODUCTION

Phospholipid-encapsulated microbubbles are routinely used as contrast agents for diagnostic ultrasound imaging because of their acoustic impedance mismatch with blood and their highly compressible nature in response to an ultrasound field (Claudon et al. 2013; Cosgrove 2006; Forsberg et al. 1998). Maximum scatter of an ultrasound wave by microbubbles occurs when the frequency of these waves is equal to the resonance frequency of the microbubbles. The size of encapsulated microbubbles is a key factor in their resonant frequency, and most commercial contrast agents (1–10 μm) have resonances within the range of frequencies used for diagnostic ultrasound imaging (Stride and Saffari 2003).

Microbubbles can undergo both linear and non-linear oscillations depending on the amplitude of the applied acoustic field (Emmer et al. 2007). Contrast imaging uses non-linear microbubble behaviour for a number of imaging techniques, such as pulse inversion, harmonic imaging and power modulation (Burns et al. 1994; Schrope and Newhouse 1993; Simpson et al. 1999). Coded excitation, such as chirps, are techniques used to increase the signal-to-noise ratio (SNR) for ultrasound imaging (Misaridis and Jensen 2005) by increasing the transited energy without decreasing the axial resolution or increasing the acoustic pressure. Longer-duration exposures can be used to increase the non-linear behaviour of microbubbles (Zhang et al. 2007), which can improve the contrast-to-tissue ratio (CTR) for contrast imaging (Harput et al. 2013; Sun et al. 2007). The response of a microbubble to an acoustic field depends on a number of factors, such as the frequency of excitation, microbubble size and shell composition (Sun et al. 2014). Generally, for low-amplitude excitation, microbubbles will oscillate linearly around their equilibrium radius, where the frequency content of the backscattered signal would be determined by the excitation waveform. Increasing the amplitude of excitation can result in non-linear oscillations of the

Address correspondence to: James R. McLaughlan, Electronic and Electrical Engineering, University of Leeds, Leeds, LS2 9JT, UK. E-mail: j.r.mclaughlan@leeds.ac.uk

microbubble, which can generate harmonics of the fundamental drive frequency (f_0) (de Jong et al. 2002). Superharmonics (nf_0) and ultraharmonics ($nf_0/2$) can be generated by non-linear oscillations, which are used to enhance ultrasound contrast imaging (de Jong et al. 2009; Maresca et al. 2013). Second harmonic ($2f_0$) emissions from microbubbles have been reported to improve the resolution of contrast-enhanced ultrasound imaging (Forsberg et al. 1997). Nevertheless, because of non-linear propagation of the ultrasound wave (Leighton 2007), a second harmonic component can be generated in tissue, which can also be used for imaging (Tranquart et al. 1999), but can reduce the performance of contrast imaging (Goertz et al. 2005; Tang et al. 2010; Yildiz et al. 2015). As subharmonic ($f_0/2$) emissions are unique to microbubble activity, they can be used to improve the CTR (Goertz et al. 2007; Shankar et al. 1998). However, it has been found that the CTR can be reduced in the region beyond a microbubble population because of the generation of the non-linear harmonics by the microbubbles that then propagate into the tissue (Tang et al. 2010). At higher acoustic amplitudes, other microbubble phenomena may occur, such as surface mode oscillations (Dollet et al. 2008) and lipid shedding. The latter could have implications for drug delivery using microbubbles (Borden et al. 2005). Further increases in the acoustic amplitude can result in the rapid expansion and collapse associated with inertial cavitation (Neppiras 1980; Prentice et al. 2005) and the destruction of the microbubble. In addition to the generation of non-linear harmonics, high-amplitude excitation can result in the generation of broadband emissions that can also be used for ultrasound contrast imaging (Gessner et al. 2010; Kruse and Ferrara 2005).

The Rayleigh–Plesset–Noltingk–Neppiras–Poritsky (RPNNP) equation is commonly used to simulate the dynamics of a free gas bubble in a liquid medium (Neppiras and Noltingk 1951; Noltingk and Neppiras 1950; Plesset 1949; Poritsky 1951; Rayleigh 1917). This equation, including its limitations (Leighton 1994), forms the basis for most theoretical models of encapsulated microbubbles (Doinikov and Bouakaz 2011). A commonly used modification of this equation for phospholipid-shelled microbubbles is the Marmottant model (Marmottant et al. 2005). This model introduces a term for effective surface tension that is dependent on the instantaneous microbubble radius, which results in three regimes for shell motion: buckled, elastic and ruptured. A consequence of this modification is the ability to then simulate large-amplitude oscillations, which can lead to non-linear behaviour in the microbubble. Such an effect has been predicted by this model and observed using high-speed imaging (de Jong et al. 2007); it is "compression-only" behaviour, which is when a microbubble, typically in a buckled state, undergoes compression in response to an ultrasound field, but very limited expansion. These non-linear oscillations can give rise to harmonic emissions from microbubbles at low acoustic pressures (Sijl et al. 2011). Subharmonic emissions generated by non-linear oscillations of phospholipid-encapsulated microbubbles are used for *in vivo* and clinical applications of diagnostic ultrasound imaging (Eisenbrey et al. 2015). These emissions required a threshold acoustic pressure to be exceeded to be generated, which is true for both free gas bubbles (Prosperetti 1976) and coated microbubbles (Sijl et al. 2010). Prosperetti described a general derivation for the acoustic pressure thresholds required for subharmonic components to be present in the acoustic emissions generated from acoustically driven gas bubbles, applied to coated bubbles (Prosperetti 2013). In this derivation it is noted that the subharmonic threshold can be lowered when compared with that of an uncoated bubble, because of the presence of discontinuities or near discontinuities in the shell of the microbubble, such as buckling.

The therapeutic application of ultrasound for cancer therapy has been widely investigated (Wood and Sehgal 2015), and the use of therapeutic microbubbles that can be targeted to specific cancerous cells holds particular promise for diagnosis and therapy (Klibanov and Hossack 2015). A common approach for the loading of therapeutics onto a microbubble is through the attachment of drug-filled liposomes to the shell of a microbubble (Geers et al. 2011; Kheirolomoom et al. 2007; Lentacker et al. 2010; Peyman et al. 2012). The ultrasonic release of a therapeutic payload from a microbubble can be achieved through its destruction (Christiansen et al. 2003; Ferrara et al. 2007; Korpanty et al. 2005; Lindner 2004; Mayer et al. 2008; Schlegel et al. 2016; Zhu et al. 2015) or through a controlled release mechanism such as phospholipid shedding (Luan et al. 2014). Nevertheless, should the microbubbles or free gas bubbles (generated from microbubble rupture) (de Jong et al. 2002; Postema et al. 2005) emit and/or re-radiate acoustic pressure in response to being driven by an acoustic field during this process, this could help increase target cell permeability through sonoporation, improving the therapeutic outcome (Delalande et al. 2013; Greenleaf et al. 1998; Kooiman et al. 2014; McLaughlan et al. 2013).

The aim of this study was to investigate the effect of liposome loading on the acoustic response of microbubble populations that were produced using a microfluidic manufacturing process (Peyman et al. 2012). The microbubble shell parameters, acoustic response and destruction thresholds were measured. In this article, the term *destruction* refers to the fragmentation of the microbubble and dissolution of the gas core (Christiansen et al. 2003; Ferrara et al. 2007).

METHODS

Microbubble and liposome manufacture

Liposomes were manufactured prior to microbubble manufacture by repeatedly extruding a phospholipid solution through a polycarbonate membrane (Olson et al. 1979). The phospholipids used in liposome manufacture were prepared by mixing DSPC, cholesterol, DSPE–PEG2000–Biotin (850365,700000 and 880129, Avanti Polar Lipids, Alabaster, AL, USA) and DHPE–Oregon Green (O-12650, Life Technologies, Paisley, UK) dissolved in chloroform, at 62.8, 32.3, 4.8 and 0.1 mol%, respectively (Abou-Saleh et al. 2013). The chloroform was evaporated under vacuum for 24 hours, after which the lipids were re-suspended in a buffer containing 1 mg/mL propidium iodide (P4864, Sigma-Aldrich, Dorset, UK), using a hot plate and vortex. However, for the purposes of this study, the fluid content of the liposomes was not important. The solution was then repeatedly passed through a mini-extruder (Avanti Polar Lipids) that was heated to 60°C to generate liposomes. Un-encapsulated propidium iodide was removed by passing the liposome solution through a column (G-25, GE Healthcare, Buckinghamshire, UK). This process produced a final concentration of 1×10^{13} liposomes/mL with a mean diameter of 200 nm.

The phospholipid solution used in microbubble production was prepared by mixing DPPC (850355, Avanti Polar Lipids) and DSPE–PEG2000–Biotin, which had been dissolved in chloroform, at 95 and 5 mol% respectively (Abou-Saleh et al. 2014). After evaporation of the chloroform, the lipids were re-suspended with a saline solution containing filtered water, 1% glycerol and 4 mg/mL NaCl, in a 1-mL vial using an ultrasound bath. A solution containing 1×10^{10} liposomes was incubated with 3 μL of NeutrAvidin (A2666, Life Technologies), a biotin-binding protein, for 20 min. This solution was then added to the 1-ml vial containing the phospholipid solution, to be used for microbubble production and incubated for an additional 20 min. This solution was then combined with (C_3F_8) gas in a multiplexed microfluidic manufacturing system for microbubble production (Peyman et al. 2012, 2016). Figure 1(a) is a schematic of the final liposome-loaded microbubble, whereas Figure 1(b) contains both dark-field and fluorescence micrographs of a microbubble population. For this example, a green fluorescent lipid was incorporated into the
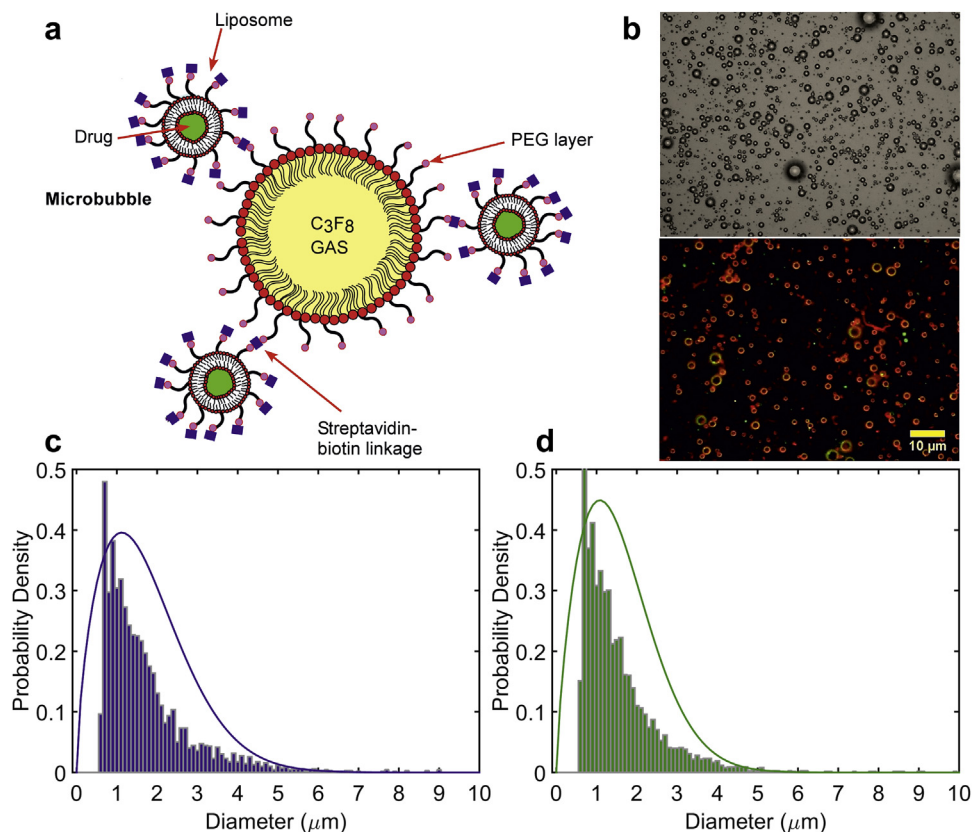

Fig. 1. (a) Schematic of the liposome-loaded microbubble (not to scale). (b) Dark-field and fluorescence microscopy images of a liposome-loaded microbubble population. (c, d) Histograms of the size ranges for (c) bare and (d) liposome-loaded microbubbles used in this study.
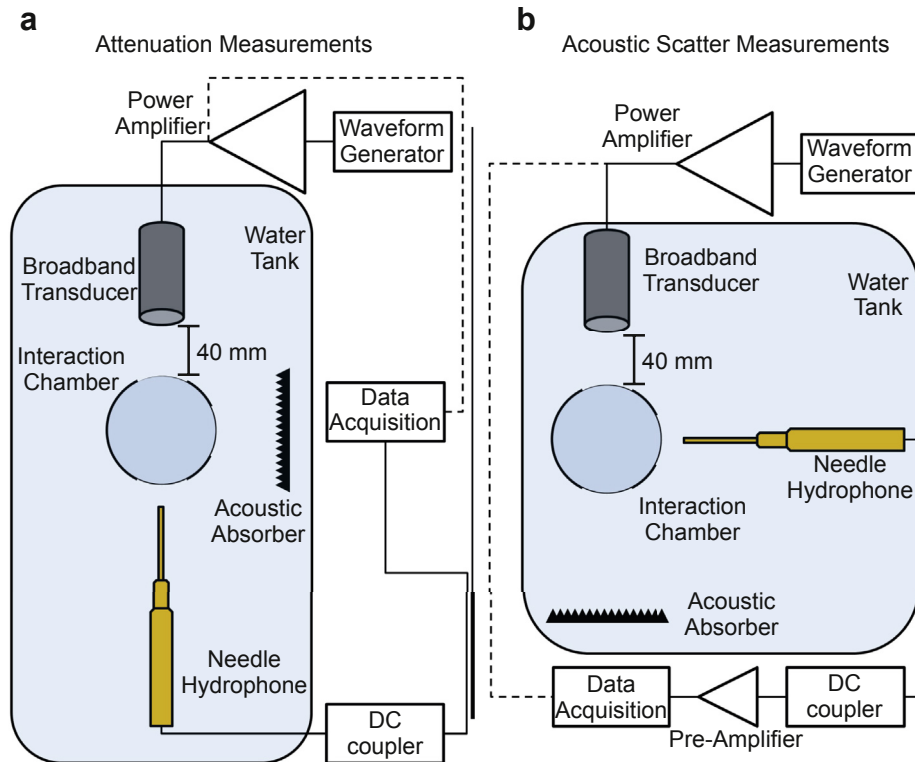
Fig. 2. Schematic of the acoustic (a) attenuation and (b) scatter experimental apparatus used in this study.

liposome shell, and a red fluorescent lipid, into the microbubble shell. The concentration and size distribution were measured optically and gave a mean diameter of 1.7 ± 1.2 μm for the liposome-loaded microbubbles and 1.6 ± 1.0 μm for the bare microbubbles (Fig. 1c, d). An average total concentration of 6 × 10^8 ± 3 × 10^8 microbubbles/mL, for both bare and liposome-loaded microbubbles was measured through five repeat preparations of each microbubble type (McLaughlan et al. 2013).

Acoustic estimation of microbubble shell parameters

Figure 2(a) is a diagram of the experimental setup used to measure the attenuation of a broadband ultrasound pulse, which propagated through an interaction chamber containing populations of either bare or liposome-loaded microbubbles. In both cases the total concentration within this chamber did not exceed 2 × 10^6 microbubbles/mL. The interaction chamber was an acrylic cylinder with an internal diameter of 30 mm; it had a total volume of 100 mL that was filled with filtered and de-ionised water, which was replaced between sample measurements. Three acoustic windows were cut into the cylinder, 20 mm in diameter, to allow direct propagation of the ultrasound beam and detection at 90° (Fig. 2). Plastic wrap 12.5 μm thick was used to seal these acoustic windows to ensure that the chamber
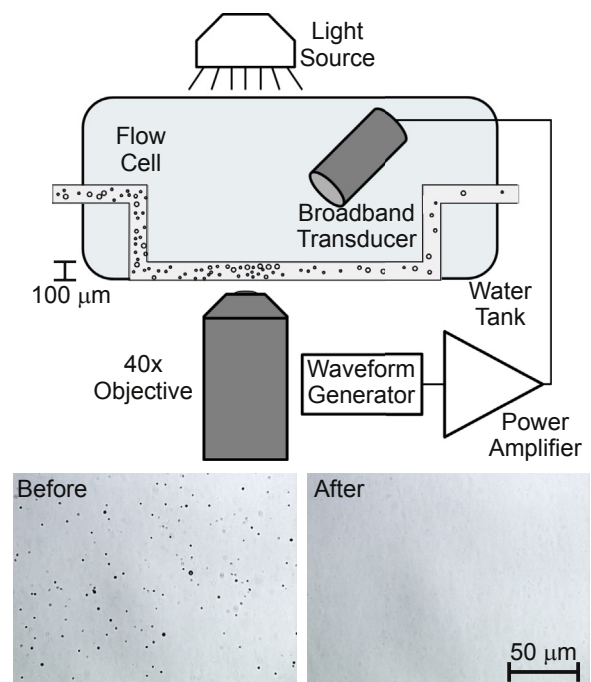

Fig. 3. Schematic of the apparatus used to measure the destruction threshold of microbubble populations, where the bright-field microscopy images reveal bubbles before and after destruction.
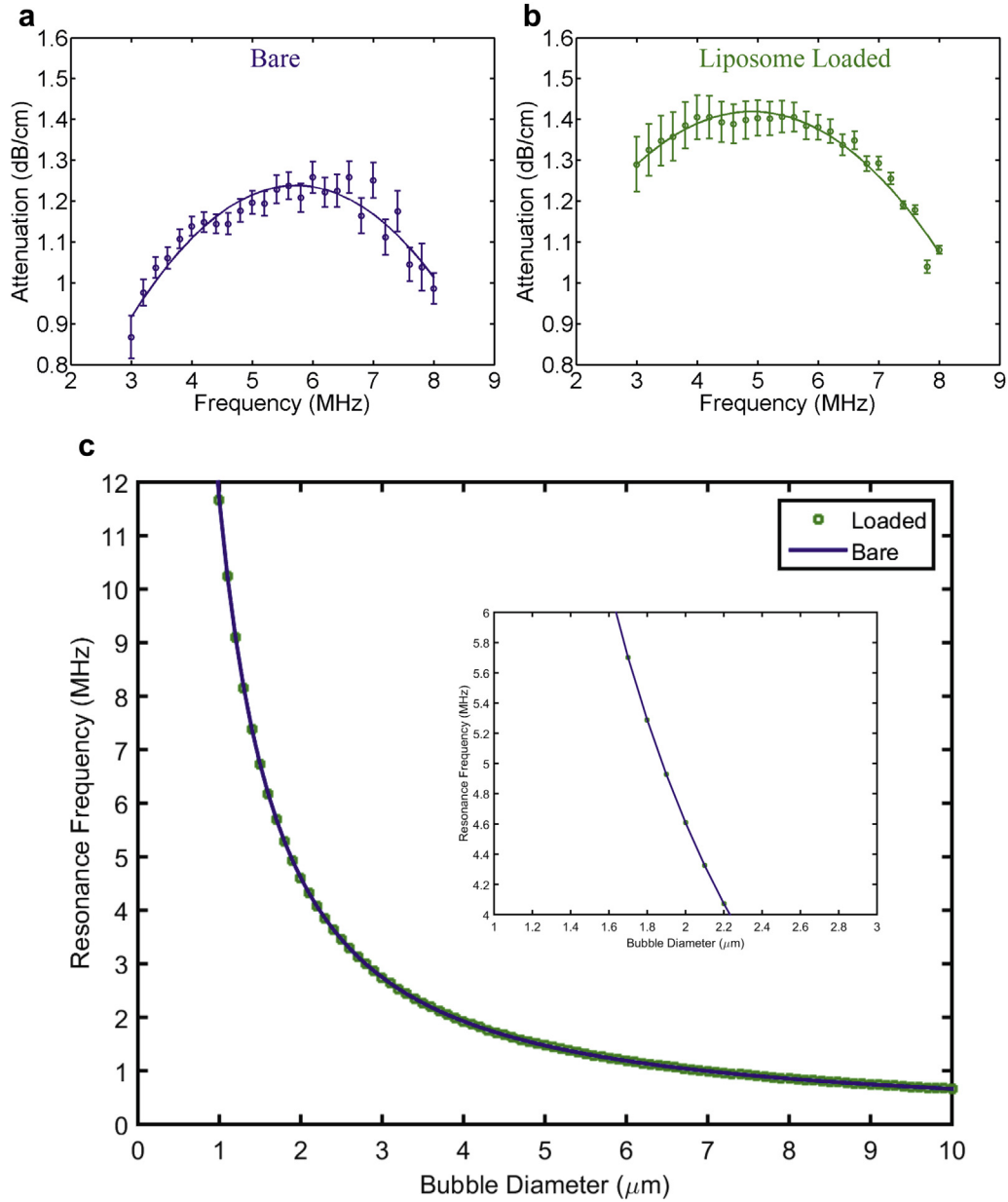
Fig. 4. Measured attenuation over the 3–8 MHz ranges of (a) bare and (b) liposome-loaded microbubbles. Error bars represent standard deviations of five repeat measurements. (c) Calculated resonant frequency for the loaded and bare microbubbles using the shell parameters in Table 1. Inset: Expanded view of these values around the mean microbubble diameter used in this study.

was watertight, but had a negligible effect on the ultrasound beam. The size of the acoustic windows ensured that the excitation pulse propagated without interaction

Table 1. Estimated shell parameters for both microbubble populations

Microbubble type	Stiffness, S_p (N/m)	Friction, S_f (10^{-6} kg/s)
Bare	0.72 ± 0.01	0.37 ± 0.05
Liposome-loaded	0.78 ± 0.05	0.74 ± 0.01

within the chamber walls. A waveform generator (33250A, Agilent Technologies, Cheshire, UK) was programmed with a 10-μs pre-distorted chirp pulse (3–8 MHz) (McLaughlan et al. 2013) that accounted for the response of the broadband transducer (V310, Olympus Industrial, Essex, UK) to provide a root mean square (RMS) peak negative pressure of 100 kPa , when driven by a power amplifier (A150, Electronics & Innovation, Rochester, NY, USA). This pressure level was chosen in an effort to operate in the linear regime of
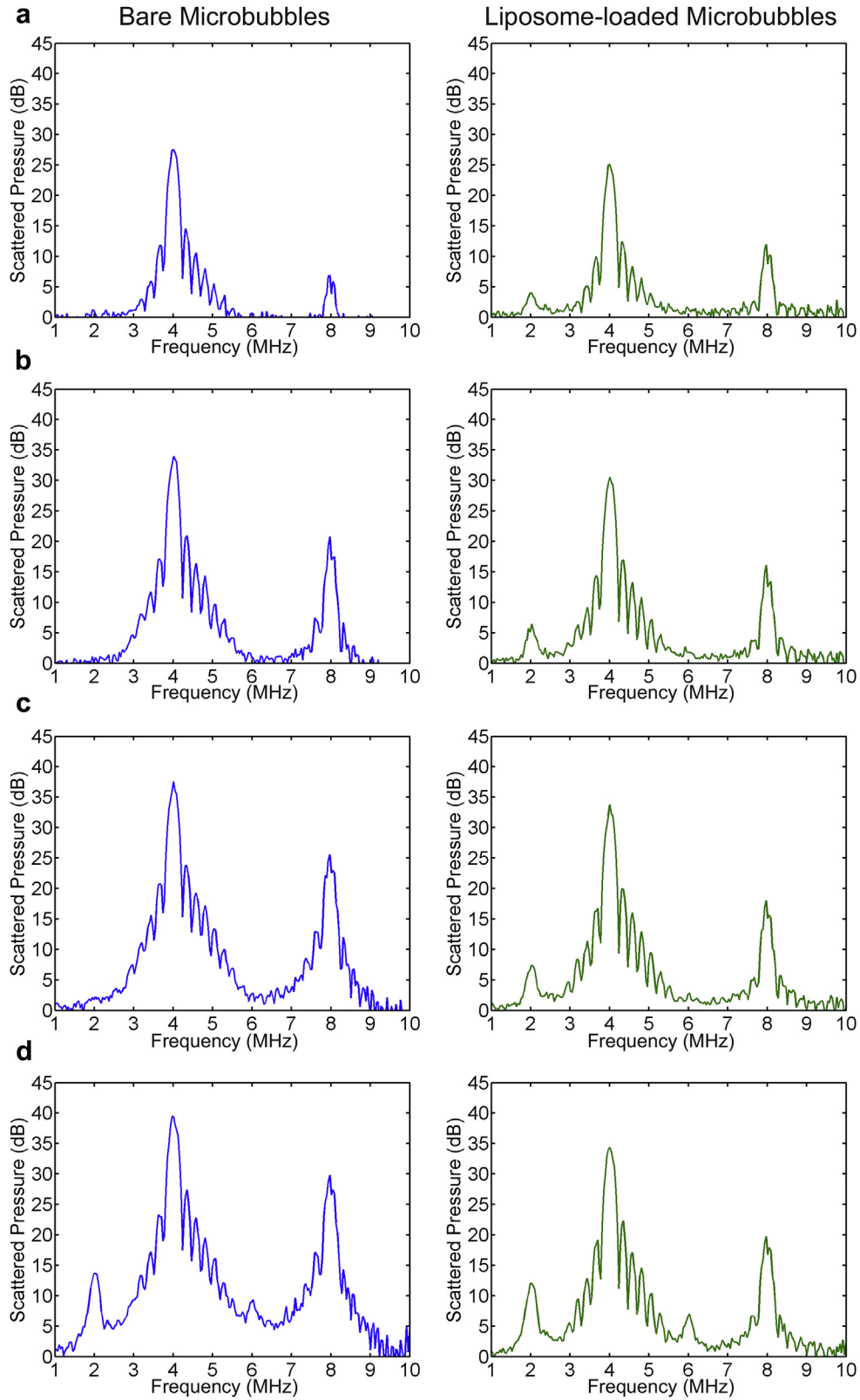
Fig. 5. Scattered acoustic spectra for (a) 50-, (b) 100-, (c) 150- and (d) 200-kPa tone bursts at 4 MHz, for both micro-bubble populations.

Subharmonic (2 MHz)

Fundamental (4 MHz)

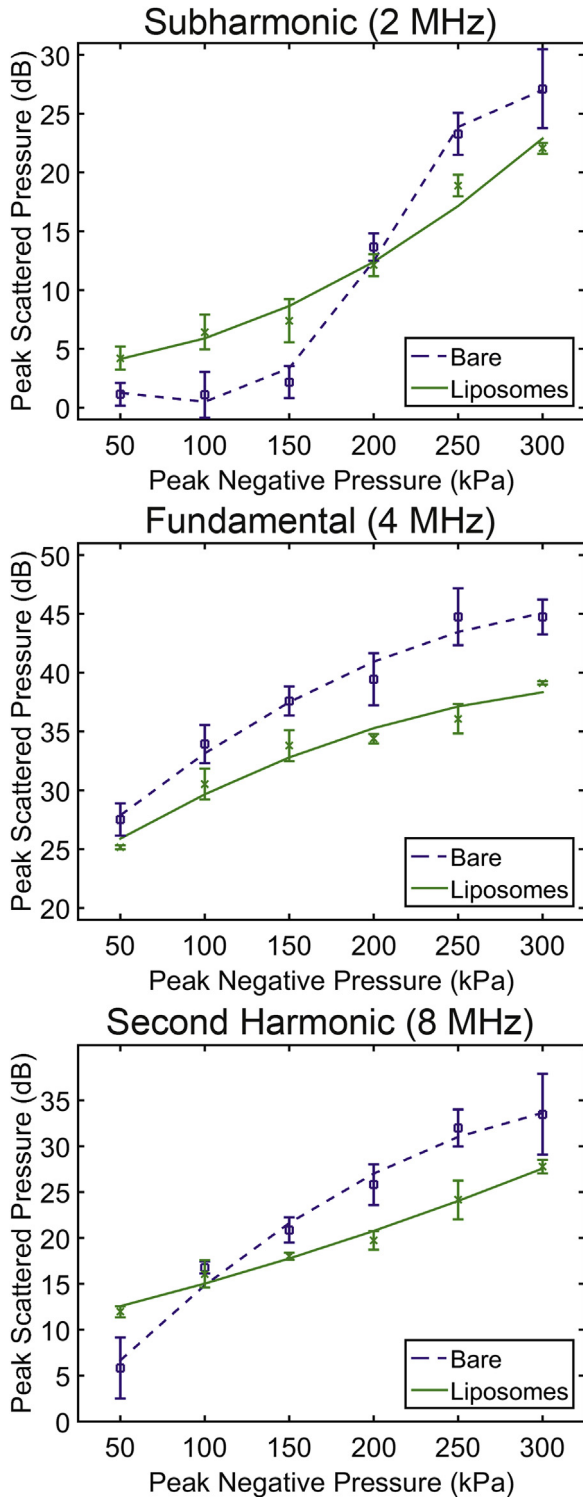
Second Harmonic (8 MHz)

Fig. 6. Averaged peak scattered pressures for subharmonic, fundamental and second harmonic components. Error bars represent the standard deviations of five repeat measurements.

microbubble population behavior, and when using a predistorted chirp it was the maximum achievable pressure level over the frequency range studied.

A 0.2-mm needle hydrophone (Precision Acoustics, Dorset, UK) was used to calibrate the output RMS pressure of the transducer, and a 1.0-mm needle hydrophone was used to measure the chirp pulses after propagating through the interaction chamber. For each sample, 500 measurements were acquired using an oscilloscope (WaveSurfer 104Xs, Teledyne LeCroy, Berkshire, UK) and downloaded to a computer for post-processing, which was repeated five times for water only and bare and liposome-loaded microbubbles. Each sequence of 500 measurements was then averaged in the frequency domain and the effect of liposome loading on the shell parameters of a microbubble population was estimated by fitting the frequency-dependent attenuation curves with theoretical predictions (de Jong et al. 1992; Faez et al. 2011; Goertz et al. 2007; Hoff et al. 2000; Raymond et al. 2014).

Acoustic detection and microbubble destruction

Figure 2(b) is a diagram of the experimental setup used to measure the acoustic scatter from populations of bare and liposome-loaded microbubbles. The apparatus used was the same as outlined in the previous section. However, for this study, the 1.0-mm hydrophone was placed perpendicular to the propagation of the ultrasound wave to detect the 90° scatter from the microbubble populations when exposed to a 10-μs 4-MHz tone burst at peak negative pressures of 50 to 300 kPa. The microbubble population in the chamber was replaced after each measurement at a given pressure level. In addition, a 40-dB pre-amplifier (5077PR, Olympus Industrial) was placed between the hydrophone and oscilloscope.

A direct comparison of the destruction threshold for bare and liposome-loaded microbubbles was performed using 2-MHz tone bursts generated by a broadband transducer (V323, Olympus Industrial), as illustrated in Figure 3, to establish if liposome loading affects this. A 2-MHz transducer was used for these measurements to maximise the available mechanical index (MI) to achieve microbubble destruction, from the electronic drive system illustrated in Figure 2. In an effort to minimise effects from primary and secondary radiation forces (Dayton et al. 1997; Doinikov and Zavtrak 1996), 10-μs ultrasound exposures with a low 10-Hz pulse repetition frequency were used to expose a low concentration (1×10^5 microbubbles/mL) of microbubbles for 1 s in a flow cell (μ-Slide VI 0.4, Ibidi, Martinsried, Germany). The transducer was aligned at 45° to the flow chamber to minimise standing waves. Bright-field microscopy images were taken before and after the ultrasound exposure using an inverted microscope (Eclipse Ti-U, Nikon UK, Surrey, UK). MATLAB (The MathWorks, Natick, MA, USA) was used for image analysis to identify the loss in the microbubble population caused by
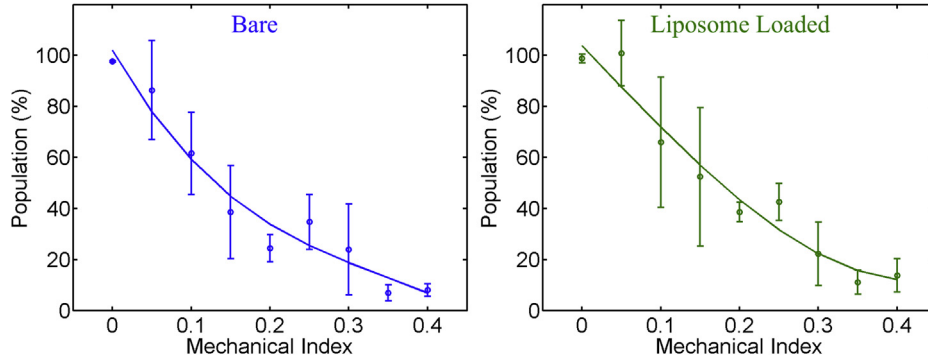
Fig. 7. Reduction in microbubble populations through single ultrasound exposures at 2 MHz. Error bars represent standard deviations of five repeat measurements.

the ultrasound exposure over a range of *in situ* peak negative pressures, or MIs (Apfel and Holland 1991; Church 2005). The MI values stated were calculated using the method that incorporated the effect of pulse duration on this parameter (Church 2005).

RESULTS

Figure 4(a, b) illustrates the attenuation (dB/cm) for these two microbubble populations measured over the range 3–8 MHz. These data were used to estimate the shell parameters of bare and liposome-loaded microbubbles in Table 1, which reveals that the shell stiffness values are equivalent and only the shell friction of the loaded microbubbles exhibits a significant increase over that of the bare microbubbles. In Figure 4(c), the calculated resonant frequency is plotted as a function of equilibrium radius. For small-amplitude oscillations (Brennen 1995), the resonant frequency, ω_r, of an encapsulated microbubble that incorporates the effects of both stiffness and viscous damping of the shell (Morgan et al. 2000) is given by

$$\omega_r^2 = \omega_0^2 - 2\beta^2$$

$$\omega_0^2 = \frac{1}{\rho R_0^2}\left[3\gamma\left(P_0 + \frac{2\sigma}{R_0} + \frac{S_p}{R_0}\right) - \frac{2\sigma}{R_0} - \frac{3S_p}{R_0}\right]$$

$$\beta = \frac{1}{\rho R_0^2}\left[2\mu + \frac{S_f}{8\pi R_0}\right]$$

where R_0 is the equilibrium radius of the microbubble (0.25–5 μm), ρ is the liquid density (998 kg/m^3), γ is the polytropic gas index (1.07), P_0 is the hydrostatic pressure (101 kPa), σ is the surface tension at the liquid–gas interface (0.0728 N/m) and μ is the liquid viscosity (0.001 Pa·s). The shell parameters for stiffness and friction are from the parameters for loaded and bare microbubbles in Table 1.

The averaged scattered acoustic pressures from 500 repeat pulses in both microbubble populations for peak negative pressures of 50–200 kPa are illustrated in Figure 5. These values are with respect to measurement taken when the chamber was filled with just filtered and de-ionised water. For both microbubble types and all acoustic pressure levels, fundamental and second harmonic components were present, the amplitude of which increases for increasing acoustic drive pressures. For liposome-loaded microbubbles a subharmonic component is present for all pressure levels that is present only at 200 kPa for the bare microbubble population.

Figure 6 gives the averaged peak components of subharmonic, fundamental and second harmonic emissions detected from both microbubble populations. For liposome-loaded microbubbles, subharmonic emissions are present for all excitation pressures. However, for bare microbubbles, subharmonic emissions are present only beyond 200 kPa. The fundamental peak for bare microbubbles is higher for all pressures used. Second harmonic emissions are detected for both microbubble populations for all exposure pressures.

The destruction of both microbubbles populations in response to a single ultrasound exposure at 2 MHz over a MI range of 0–0.4 is illustrated in Figure 7. For an MI greater than 0.4 (570 kPa), 80% of both populations were destroyed.

DISCUSSION

For drug-loaded microbubbles to be realised as therapeutic agents, it is important that their response under ultrasound exposure be investigated. In this study, a number of complementary characterisation techniques were performed on microbubbles that were generated using a microfluidic manufacturing process (Peyman et al. 2012). In all cases a direct comparison between liposome-loaded and bare microbubbles was made such that the shell

composition, gas core and mean diameter were equivalent.

The average shell stiffness and friction of the microbubble populations were measured using acoustic attenuation methods routinely used for the characterisation of ultrasound contrast agents. This indicated that the shell stiffness values of these microfluidic generated microbubbles were not affected by the attachment of liposomes and were consistent with those values previously reported (Peyman et al. 2012). However, these values were slightly lower than those of the commercial agents SonoVue and Definity (Faez et al. 2011). The shell friction for liposome-loaded microbubbles doubled, which is consistent with observed measurements through high speed photography (Luan et al. 2012). In their study, Luan et al. proposed that the increased shell friction, or viscosity, was due predominately to the interactions between liposomes during microbubble oscillations. It was also observed that liposome-loaded microbubbles exhibited "expansion-only" behaviour at acoustic pressures below 30 kPa, whereas this type of behavior, where a microbubble would undergo very little or no compression, was previously observed at high acoustic pressures (Emmer et al. 2007). If it is assumed that the liposomes form a uniform closely packed layer around the microbubble (Geers et al. 2011), then the equilibrium radius of the bubble R_0 would be effectively equivalent or close to the buckling radius R_b (Marmottant et al. 2005). This enforced buckled state would then lead to minimal compression in the microbubble, which would result in expansion-only behaviour occurring at low acoustic pressures in liposome-loaded microbubbles when compared with bare microbubbles. Thus, the presence of liposomes causes a discontinuity in the shell of the microbubble, which has been proposed as a cause of reduced subharmonic threshold (Prosperetti 2013), and is the likely cause of the observed decrease in the subharmonic threshold in this study, as illustrated by the acoustic spectra in Figure 5. A similar effect has been simulated with the introduction of gold nanoparticles into the shell of a microbubble, thus restricting its ability to compress (Stride et al. 2008). The average subharmonic peak scattered pressure illustrated in Figure 6 indicates that at pressures ≥200 kPa, both microbubble types exceeded the subharmonic threshold and bare microbubbles had an increased amplitude beyond this level. The extra damping, caused by an increased shell friction for the loaded bubbles, is the likely reason for this difference. Thus, once the subharmonic threshold for the bare microbubbles was exceeded, the amplitude of these detected emissions was generally higher (Fig. 6) than that for the equivalent liposome-loaded microbubbles.

A number of release mechanisms for drug-loaded microbubbles are possible (Klibanov et al. 2010; Kooiman et al. 2014; Meijering et al. 2009); however,

for targeted liposome-loaded microbubbles (Peyman et al. 2012), the release mechanism will likely be microbubble destruction. In the absence of sonoporation, the drug-loaded liposomes would then deliver their therapeutic payload to the targeted cell population through endocytosis (Torchilin 2005). To assess if attaching liposomes to the shells of these microfluidic generated microbubbles affects their destruction threshold, a microscopy-based technique for assessing this was implemented (Fig. 3), and it was found that there was no difference between the destruction thresholds of these bare and liposome-loaded microbubbles (Fig. 7). Molecular-targeted therapeutic microbubbles hold significant promise for the identification and treatment of diseases, such as cancer (Ibsen et al. 2013). Nevertheless, for contrast-enhanced ultrasound imaging, subharmonic emissions from microbubbles remain the only uniquely identifiable signal and would thus be most suitable for molecular imaging applications.

CONCLUSIONS

In this study, acoustic characterisation of microfluidic manufactured microbubble populations, which were either bare or liposome loaded, was performed to assess the effect that addition of a therapeutic payload may have on their acoustic response. It was found that liposome loading had a minimal effect on microbubble shell stiffness and their acoustic destruction threshold. An increase in shell friction was observed for the liposome-loaded microbubble population. The acoustic pressure threshold for the production of subharmonic emissions was significantly lower for the liposome-loaded microbubbles than equivalent bare microbubbles. Attachment of a therapeutic payload to a microbubbles via liposome loading will improve their ability to perform molecular imaging using subharmonic emissions, and combined with a single-step microfluidic manufacturing process, it could lead to therapeutic microbubbles making an important contribution to the identification and treatment of cancer.

REFERENCES

Abou-Saleh RH, Peyman SA, Critchley K, Evans SD, Thomson NH. Nanomechanics of lipid encapsulated microbubbles with functional coatings. Langmuir 2013;29:4096–4103.
Abou-Saleh RH, Swain M, Evans SD, Thomson NH. Poly (ethylene glycol) lipid-shelled microbubbles: abundance, stability, and mechanical properties. Langmuir 2014;30:5557-55563.

Apfel RE, Holland CK. Gauging the likelihood of cavitation from short-pulse, low-duty cycle diagnostic ultrasound. Ultrasound Med Biol 1991;17:179–185.

Borden MA, Kruse DE, Caskey CF, Zhao S, Dayton PA, Ferrara KW. Influence of lipid shell physicochemical properties on ultrasound-induced microbubble destruction. IEEE Trans Ultrason Ferroelectr Freq Control 2005;52:1992–2002.

Brennen CE. Cavitation and bubble dynamics. New York/London: Oxford University Press; 1995.

Burns P, Powers J, Simpson D, Brezina A, Kolin A, Chin C, Uhlendorf V, Fritzsch T. Harmonic power mode Doppler using microbubble contrast agents: An improved method for small vessel flow imaging. Proc IEEE Ultrason Symp 1994;3:1547–1550.

Christiansen JP, French BA, Klibanov AL, Kaul S, Lindner JR. Targeted tissue transfection with ultrasound destruction of plasmid-bearing cationic microbubbles. Ultrasound Med Biol 2003;29:1759–1767.

Church CC. Frequency, pulse length, and the mechanical index. Acoust Res Lett Online 2005;63:162–168.

Claudon M, Dietrich CF, Choi BI, Cosgrove DO, Kudo M, Nolse CP, Piscaglia F, Wilson SR, Barr RG, Chammas MC, Chaubal NG, Chen MH, Clevert DA, Correas JM, Ding H, Forsberg F, Fowlkes JB, Gibson RN, Goldberg BB, Lassau N, Leen EL, Mattrey RF, Moriyasu F, Solbiati L, Weskott HP, Xu HX. Guidelines and good clinical practice recommendations for contrast enhanced ultrasound (CEUS) in the liver—Update 2012: A WFUMB-EFSUMB initiative in cooperation with representatives of AFSUMB, AIUM, ASUM, FLAUS and ICUS. Ultrasound Med Biol 2013;39:187–210.

Cosgrove D. Ultrasound contrast agents: An overview. Eur J Radiol 2006;60:324–330.

Dayton P, Morgan K, Klibanov A, Brandenburger G, Nightingale K, Ferrara K. A preliminary evaluation of the effects of primary and secondary radiation forces on acoustic contrast agents. IEEE Trans Ultrason Ferroelectr Freq Control 1997;44:1264–1277.

de Jong N, Bouakaz A, Frinking P. Basic acoustic properties of microbubbles. Echocardiography 2002;19:229–240.

de Jong N, Emmer M, Chin CT, Bouakaz A, Mastik F, Lohse D, Versluis M. 'Compression-only' behavior of phospholipid-coated contrast bubbles. Ultrasound Med Biol 2007;33:653–656.

de Jong N, Emmer M, Wamel A, Versluis M. Ultrasonic characterization of ultrasound contrast agents. Med Biol Eng Comput 2009;47:861–873.

de Jong N, Hoff L, Skotland T, Bom N. Absorption and scatter of encapsulated gas filled microspheres: Theoretical considerations and some measurements. Ultrasonics 1992;30:95–103.

Delalande A, Kotopoulis S, Postema M, Midoux P, Pichon C. Sonoporation: Mechanistic insights and ongoing challenges for gene transfer. Gene 2013;525:191–199.

Doinikov AA, Bouakaz A. Review of shell models for contrast agent microbubbles. IEEE Trans Ultrason Ferroelectr Freq Control 2011;58:981–993.

Doinikov AA, Zavtrak ST. On the "bubble grapes" induced by a sound field. J Acoust Soc Am 1996;99:3849–3850.

Dollet B, Van Der Meer SM, Garbin V, De Jong N, Lohse D, Versluis M. Nonspherical oscillations of ultrasound contrast agent microbubbles. Ultrasound Med Biol 2008;34:1465–1473.

Eisenbrey JR, Sridharan A, Liu JB, Forsberg F. Recent experiences and advances in contrast-enhanced subharmonic ultrasound. BioMed Res Int 2015;2015:640397.

Emmer M, Van Wamel A, Goertz DE, De Jong N. The onset of microbubble vibration. Ultrasound Med Biol 2007;33:941–949.

Faez T, Goertz D, De Jong N. Characterization of Definity ultrasound contrast agent at frequency range of 5–15 MHz. Ultrasound Med Biol 2011;37:338–342.

Ferrara K, Pollard R, Borden M. Ultrasound microbubble contrast agents: Fundamentals and application to gene and drug delivery. Annu Rev Biomed Eng 2007;91:415–447.

Forsberg F, Goldberg BB, Wu Y, Liu JB, Merton DA, Rawool NM. Harmonic imaging with gas-filled microspheres: Initial experiences. Int J Imaging Systems Technol 1997;8:69–81.

Forsberg F, Merton D, Liu J, Needleman L, Goldberg B. Clinical applications of ultrasound contrast agents. Ultrasonics 1998;36:695–701.

Geers B, Lentacker I, Sanders NN, Demeester J, Meairs S, De Smedt SC. Self-assembled liposome-loaded microbubbles: The missing link for safe and efficient ultrasound triggered drug-delivery. J Control Release 2011;152:249–256.

Gessner R, Lukacs M, Lee M, Cherin E, Foster F, Dayton P. High-resolution, high-contrast ultrasound imaging using a prototype dual-frequency transducer: In vitro and in vivo studies. IEEE Trans Ultrason Ferroelectr Freq Control 2010;57:1772–1781.

Goertz DE, Cherin E, Needles A, Karshafian R, Brown AS, Burns PN, Foster FS. High frequency nonlinear B-scan imaging of microbubble contrast agents. IEEE Trans Ultrason Ferroelectr Freq Control 2005;52:65–79.

Goertz DE, Frijlink ME, Tempel D, Bhagwandas V, Gisolf A, Krams R, de Jong N, van der Steen AF. Subharmonic contrast intravascular ultrasound for vasa vasorum imaging. Ultrasound Med Biol 2007;33:1859–1872.

Greenleaf WJ, Bolander ME, Sarkar G, Goldring MB, Greenleaf JF. Artificial cavitation nuclei significantly enhance acoustically induced cell transfection. Ultrasound Med Biol 1998;24:587–595.

Harput S, Arif M, McLaughlan J, Cowell DMJ, Freear S. The effect of amplitude modulation on subharmonic imaging with chirp excitation. IEEE Trans Ultrason Ferroelectr Freq Control 2013;60:2532–2544.

Hoff L, Sontum PC, Hovem JM. Oscillations of polymeric microbubbles: Effect of the encapsulating shell. J Acoust Soc Am 2000;107:2272–2280.

Ibsen S, Schutt CE, Esener S. Microbubble-mediated ultrasound therapy: A review of its potential in cancer treatment. Drug Design Dev Ther 2013;7:375.

Kheirolomoom A, Dayton PA, Lum AF, Little E, Paoli EE, Zheng H, Ferrara KW. Acoustically-active microbubbles conjugated to liposomes: Characterization of a proposed drug delivery vehicle. J Control Release 2007;118:275–284.

Klibanov AL, Hossack JA. Ultrasound in radiology: From anatomic, functional, molecular imaging to drug delivery and image-guided therapy. Invest Radiol 2015;50:657–670.

Klibanov AL, Shevchenko TI, Raju BI, Seip R, Chin CT. Ultrasound-triggered release of materials entrapped in microbubble liposome constructs: A tool for targeted drug delivery. J Control Release 2010;148:13–17.

Kooiman K, Vos R, Versluis M, de Jong N. Acoustic behavior of microbubbles and implications for drug delivery. Adv Drug Deliv Rev 2014;72:28–48.

Korpanty G, Chen S, Shohet R, Ding JH, Yang BZ, Frenkel P, Grayburn P. Targeting of vegf-mediated angiogenesis to rat myocardium using ultrasonic destruction of microbubbles. Gene Ther 2005;12:1305–1312.

Kruse DE, Ferrara KW. A new imaging strategy using wideband transient response of ultrasound contrast agents. IEEE Trans Ultrason Ferroelectr Freq Control 2005;52:1320–1329.

Leighton TG. The acoustic bubble. New York: Academic Press; 1994.

Leighton TG. What is ultrasound? Prog Biophys Mol Biol 2007;93:3–83.

Lentacker I, Geers B, Demeester J, De Smedt SC, Sanders NN. Design and evaluation of doxorubicin-containing microbubbles for ultrasound-triggered doxorubicin delivery: cytotoxicity and mechanisms involved. Mol Ther 2010;18:101–108.

Lindner JR. Microbubbles in medical imaging: current applications and future directions. Nat Rev Drug Discov 2004;3:527–533.

Luan Y, Faez T, Gelderblom E, Skachkov I, Geers B, Lentacker I, van der Steen T, Versluis M, de Jong N. Acoustical properties of individual liposome-loaded microbubbles. Ultrasound Med Biol 2012;38:2174–2185.

Luan Y, Lajoinie G, Gelderblom E, Skachkov I, van der Steen AF, Vos HJ, Versluis M, De Jong N. Lipid shedding from single oscillating microbubbles. Ultrasound Med Biol 2014;40:1834–1846.

Maresca D, Renaud G, van Soest G, Li X, Zhou Q, Shung KK, de Jong N, van der Steen AF. Contrast-enhanced intravascular ultrasound pulse sequences for bandwidth-limited transducers. Ultrasound Med Biol 2013;39:706–713.

Marmottant P, van der Meer S, Emmer M, Versluis M, de Jong N, Hilgenfeldt S, Lohse D. A model for large amplitude oscillations of coated bubbles accounting for buckling and rupture. J Acoust Soc Am 2005;118:3499–3505.

Mayer CR, Geis NA, Katus HA, Bekeredjian R. Ultrasound targeted microbubble destruction for drug and gene delivery. Expert Opin Drug Deliv 2008;5:1121–1138.

McLaughlan J, Ingram N, Smith PR, Harput S, Coletta PL, Evans S, Freear S. Increasing the sonoporation efficiency of targeted polydisperse microbubble populations using chirp excitation. IEEE Trans Ultrason Ferroelectr Freq Control 2013;60: 2511–2520.

Meijering BD, Juffermans LJ, van Wamel A, Henning RH, Zuhorn IS, Emmer M, Versteilen AM, Paulus WJ, van Gilst WH, Kooiman K, de Jong N, Musters RJ, Deelman LE, Kamp O. Ultrasound and microbubble-targeted delivery of macromolecules is regulated by induction of endocytosis and pore formation. Circ Res 2009;104: 679–687.

Misaridis T, Jensen J. Use of modulated excitation signals in medical ultrasound: Part I. basic concepts and expected benefits. IEEE Trans Ultrason Ferroelectr Freq Control 2005;52:177–191.

Morgan K, Allen J, Dayton P, Chomas J, Klibanov A, Ferrara K. Experimental and theoretical evaluation of microbubble behavior: Effect of transmitted phase and bubble size. IEEE Trans Ultrason Ferroelectr Freq Control 2000;47:1494–1509.

Neppiras EA. Acoustic cavitation. Phys Rep 1980;61:159–251.

Neppiras EA, Noltingk BE. Cavitation produced by ultrasonics: Theoretical conditions for the onset of cavitation. Proc Phys Soc. Sect B 1951;64:1032–1038.

Noltingk BE, Neppiras EA. Cavitation produced by ultrasonics. Proc Phys Soc Sect B 1950;63:674–685.

Olson F, Hunt C, Szoka F, Vail W, Papahadjopoulos D. Preparation of liposomes of defined size distribution by extrusion through polycarbonate membranes. Biochim Biophys Acta Biomembranes 1979; 557:9–23.

Peyman SA, Abou-Saleh RH, McLaughlan JR, Ingram N, Johnson BRG, Critchley K, Freear S, Evans JA, Markham AF, Coletta PL, Evans SD. Expanding 3D geometry for enhanced on-chip microbubble production and single step formation of liposome modified microbubbles. Lab Chip 2012;12:4544–4552.

Peyman SA, McLaughlan JR, Abou-Saleh RH, Marston G, Johnson BR, Freear S, Coletta PL, Markham AF, Evans SD. On-chip preparation of nanoscale contrast agents towards high-resolution ultrasound imaging. Lab Chip 2016;16:679–687.

Plesset M. The dynamics of cavitation bubbles. J Appl Mech 1949;16: 277–282.

Poritsky H. The collapse or growth of a spherical bubble or cavity in a viscous fluid. In: Proceedings, First U.S. National Congress of Applied Mechanics held at the Illinois Institute of Technology, June 11–16, 1951. New York: American Society of Mechanical Engineers; 1951. p. 813–821.

Postema M, Bouakaz A, Versluis M, De Jong N. Ultrasound-induced gas release from contrast agent microbubbles. IEEE Trans Ultrason Ferroelectr Freq Control 2005;52:1035–1041.

Prentice P, Cuschieri A, Dholakia K, Prausnitz M, Campbell P. Membrane disruption by optically controlled microbubble cavitation. Nat Phys 2005;12:107–110.

Prosperetti A. Subharmonics and ultraharmonics in the forced oscillations of weakly nonlinear systems. Am J Phys 1976;44:548–554.

Prosperetti A. A general derivation of the subharmonic threshold for non-linear bubble oscillations. J Acoust Soc Am 2013;133: 3719–3726.

Rayleigh L. On the pressure developed in a liquid during the collapse of a spherical cavity. Phil Mag 1917;34:94–98.

Raymond JL, Haworth KJ, Bader KB, Radhakrishnan K, Griffin JK, Huang SL, McPherson DD, Holland CK. Broadband attenuation measurements of phospholipid-shelled ultrasound contrast agents. Ultrasound Med Biol 2014;40:410–421.

Schlegel P, Huditz R, Meinhardt E, Rapti K, Geis N, Most P, Katus HA, Müller OJ, Bekeredjian R, Raake PW. Locally targeted cardiac gene delivery by AAV microbubble destruction in a large animal model. Hum Gene Ther methods 2016;27:71–78.

Schrope BA, Newhouse VL. Second harmonic ultrasonic blood perfusion measurement. Ultrasound Med Biol 1993;19:567–579.

Shankar P, Krishna PD, Newhouse V. Advantages of subharmonic over second harmonic backscatter for contrast-to-tissue echo enhancement. Ultrasound Med Biol 1998;24:395–399.

Sijl J, Dollet B, Overvelde M, Garbin V, Rozendal T, de Jong N, Lohse D, Versluis M. Subharmonic behavior of phospholipid-coated ultrasound contrast agent microbubbles. J Acoust Soc Am 2010;128:3239–3252.

Sijl J, Overvelde M, Dollet B, Garbin V, De Jong N, Lohse D, Versluis M. Compression-only behavior: A second-order nonlinear response of ultrasound contrast agent microbubbles. J Acoust Soc Am 2011;129:1729–1739.

Simpson D, Chin CT, Burns P. Pulse inversion Doppler: A new method for detecting nonlinear echoes from microbubble contrast agents. IEEE Trans Ultrason Ferroelectr Freq Control 1999;46:372–382.

Stride E, Pancholi K, Edirisinghe M, Samarasinghe S. Increasing the nonlinear character of microbubble oscillations at low acoustic pressures. J R Soc Interface 2008;5:807–811.

Stride E, Saffari N. Microbubble ultrasound contrast agents: a review. Proc Inst Mech Eng H 2003;217:429–447.

Sun C, Sboros V, Butler MB, Moran CM. In vitro acoustic characterization of three phospholipid ultrasound contrast agents from 12 to 43 MHz. Ultrasound Med Biol 2014;40:541–550.

Sun Y, Kruse D, Ferrara K. Contrast imaging with chirped excitation. IEEE Trans Ultrason Ferroelectr Freq Control 2007;54:520–529.

Tang MX, Kamiyama N, Eckersley RJ. Effects of nonlinear propagation in ultrasound contrast agent imaging. Ultrasound Med Biol 2010;36: 459–466.

Torchilin VP. Recent advances with liposomes as pharmaceutical carriers. Nat Rev Drug Discov 2005;42:145–160.

Tranquart F, Grenier N, Eder V, Pourcelot L. Clinical use of ultrasound tissue harmonic imaging. Ultrasound Med Biol 1999;25:889–894.

Wood AK, Sehgal CM. A review of low-intensity ultrasound for cancer therapy. Ultrasound Med Biol 2015;4:905–928.

Yildiz YO, Eckersley RJ, Senior R, Lim AK, Cosgrove D, Tang MX. Correction of non-linear propagation artifact in contrast-enhanced ultrasound imaging of carotid arteries: Methods and in vitro evaluation. Ultrasound Med Biol 2015;41:1938–1947.

Zhang D, Gong Y, Gong X, Liu Z, Tan K, Zheng H. Enhancement of subharmonic emission from encapsulated microbubbles by using a chirp excitation technique. Phys Med Biol 2007;52:5531.

Zhu F, Jiang Y, Luo F, Li P. Effectiveness of localized ultrasound-targeted microbubble destruction with doxorubicin liposomes in H22 mouse hepatocellular carcinoma model. J Drug Target 2015; 23:323–334.